Visual Abstract

Fracture Load Estimations for U-Notched and V-Notched 3D Printed PLA and Graphene-Reinforced PLA plates using the ASED Criterion

Marcos Sánchez, Sergio Arrieta, Sergio Cicero
LADICIM (Laboratory of Materials Science and Engineering), Universidad de Cantabria, ETS de Ingenieros de Caminos, Canales y Puertos, Av. Los Castros 44, Santander 39005, Spain
marco.sanchez@unican.es, sergio.arrieta@unican.es, sergio.cicero@unican.es

ABSTRACT. This paper addresses the estimation of critical loads in FFF (Fused Filament Fabrication) printed polymers and composites containing notches. Particularly, the analysis is focused on the fracture load estimations of 39 PLA (polylactic acid) and 39 graphene reinforced PLA (PLA-Gr) printed plates containing two different types of notches (U- and V-notches) and combining different plate thicknesses and defect length to plate width (a/W) ratios. The addition of graphene (1 wt.%) increases both the yield stress and the ultimate tensile strength, also reducing the strain at rupture and, thus, generating a material whose behavior is closer to linear elasticity. Among the different assessment tools that may be used to estimate critical loads, this work applies the well-known Averaged Strain Energy Density (ASED) criterion, which compares the averaged strain energy over a certain control volume at the notch tip with the corresponding critical value, the latter being a material property. This approach has a linear-elastic nature, so its application to non-fully linear materials may require the use of specific corrections or calibrations. For the two materials analyzed here, PLA and PLA-Gr, it has been observed that the ordinary linear-elastic ASED criterion provides good estimations for the PLA-Gr material, whereas the pristine PLA, with more evident non-linear behavior, the obtainment of accurate results requires a previous specific calibration of the ASED material parameters.

KEYWORDS. Fracture, PLA, Graphene, Plate, Additive manufacturing, Notch, ASED.

OPEN ACCESS

Citation: Sánchez, M., Arrieta, S., Cicero, S., Fracture Load Estimations for U-Notched and V-Notched Specimens in 3D Printed PLA and Graphene-Reinforced PLA using the ASED Criterion, Frattura ed Integrità Strutturale, 66 (2023) 322-338.

Received: 29.08.2023
Accepted: 11.09.2023
Online first: 26.09.2023
Published: 01.10.2023

INTRODUCTION

Fused Filament Fabrication (FFF) is a fabrication technique that allows complex shapes to be created and may be applied to a wide range of materials, including polymers, metals, ceramics, and composites. The FFF technology involves the process of extruding a melted filament through a heated nozzle. This filament is subsequently placed onto a build platform layer by layer until the complete component is manufactured [1]. Currently, and particularly for the case of polymers and polymer-matrix composites, FFF has been applied to prototyping of components, but not to generate (structural) components sustaining loads as one of their main tasks. The main reason for this is that the obtained mechanical properties are generally inferior to those achieved by other well-known manufacturing methods such as injection, extrusion, or blow molding. Currently, combining the potential of the FFF technology with its main limitations, there are remarkable research efforts to develop a better understanding of this 3D printing technique and to improve the mechanical properties of the resulting printed materials (e.g., [1–6]). Understanding how these materials behave under different types of loadings and developing reliable tools to estimate the resulting critical loads are key dimensions for the use of FFF materials in structural applications.

On the other hand, it is important to note that 3D printed components commonly exhibit regions of elevated stress concentrations. These areas, known as stress risers, can be for example flaws generated during the manufacturing process (e.g., pores), defects caused by operational damage (e.g., dents), or geometrical details intentionally integrated in the design itself (e.g., holes, grooves, corners). Such defects determine the structural integrity of the corresponding component, as they may be the source of critical crack propagation causing the final fracture, or initiators of subcritical processes (e.g., fatigue) that also may lead to the final failure. Anyhow, these defects are not generally crack-like defects (i.e., infinitely sharp) and require specific approaches when evaluating the structural integrity, given that the application of traditional crack assessment methodologies would generally lead to overconservative results.

To enhance the accuracy of fracture load predictions in the presence of notches, diminishing the above-mentioned conservatism, a number of methods have been proposed in recent years. The scientific community has made considerable progress in establishing theories and methods to better understand the fracture behavior in notched components. Notably, but not only, the Theory of Critical Distances (TCD) [7] and the Average Strain Energy Density (ASED) criterion [8–11] are two widely utilized approaches that have been successful in analyzing a variety of materials and loading situations.

In this sense, the linear-elastic formulation of the ASED criterion may exhibit important limitations to provide accurate predictions of the fracture behavior of non-fully linear materials, whereas the TCD has been successfully calibrated to evaluate non-linear situations through the corresponding calibration of the critical distance [7]. Consequently, researchers have examined a number of strategies to increase the applicability of the ASED criterion to materials that develop non-linear behavior. These strategies involve combining the traditional ASED criterion with some cutting-edge ideas [12,13] like the Fictitious Material Concept (FMC) [12], or the Equivalent Material Concept (EMC) [13], among others. These alternatives substitute the actual non-linear material by a fictitious or equivalent material, respectively, that develops linear-elastic behavior and, thus, may be analyzed through linear-elastic approaches. These alternative approaches frequently involve additional steps to estimate fracture loads, which can complicate the analysis.

In the present study, a calibration technique is employed to predict fracture loads using the ASED criterion without requiring such additional steps. So far, and to the knowledge of the authors, this calibration approach has been successfully applied only in conventional fracture mechanic specimens (e.g., compact tension or single edge notch bend specimens) [14]. However, this work presents the analysis of fracture loads in FFF printed PLA (polylactic acid) and graphene-reinforced PLA (PLA-Gr) plates containing U and V-shaped notches. A total of 78 plates per material were printed and subsequently tested, combining the two analyzed materials, the two types of notches (U and V), and different plate thicknesses and notch length to plate width (a/W) ratios, obtaining the corresponding critical loads under pure tensile mode loading. Then, the ASED criterion was applied to obtain estimations of the critical loads, with the corresponding material parameters derived from both the ASED linear-elastic formulation and a specific calibration process. Finally, the experimental values and the ASED estimations are compared. These contents are presented through the following sections: Materials and Methods, describing the two materials analyzed in this work, the fabrication process and printing parameters, the resulting plate geometries, the proper testing process of the plates with the corresponding experimental critical loads, the ASED criterion in the two referred versions (linear-elastic and calibrated), and the finite element (FE) simulation performed to determine the stress fields at the notch tips; Results and Discussion, gathering the predictions of critical loads provided by the ASED criterion, their comparison with the corresponding experimental values, and the analysis of the accuracy of the ASED criterion without and with calibration process in the two materials being analyzed; and, Conclusions, gathering the main findings of this research and pointing out the limitations and possibilities of the ASED criterion to provide critical loads in both FFF printed PLA and PLA-Gr.

MATERIALS AND METHODS

The mechanical properties of FFF printed materials have gained significant interest due to widespread applications. In this study, we focus on PLA and PLA-Gr, the latter being graphene-additivated (1 wt.%) PLA. A previous work of the authors has already examined the basic tensile and fracture properties of these two materials [15]. Here, the investigation was extended by analyzing the behavior of structural plates containing different types of notches.
The PLA and PLA-Gr plates were manufactured using an FFF-based Prusa i3 printer with a raster orientation of 45/-45, employing the same specific printing parameters reported in [15] for the tensile and SENB fracture specimens used in the basic characterization. The nozzle diameter was 0.4 mm, and the nozzle temperature was set at 200 °C, while the bed temperature was maintained at 75 °C. The printing rate was 30 mm/s, and the infill level was set at 100%. Layer height was maintained at 0.3 mm.
The tensile tests reported in [15] followed ASTM D638 [16], whereas fracture tests on both cracked and notched specimens followed ASTM D6068 [17], as reported in [18]. The main mechanical properties derived from the tensile specimens and the cracked fracture specimens are gathered in Tab. 1 [15,18], while Fig. 1 shows examples of the obtained stress-strain curves revealing how PLA-Gr material develops a stress-strain curve which is much closer to linear-elastic conditions than that developed by PLA.

Material	Raster orientation	E (MPa)	σ_y (MPa)	σ_u (MPa)	ε_u (%)	K_{mat} (MPa·m$^{0.5}$)
PLA	45/-45	2751 ± 406	35.3 ± 4.6	41.1 ± 5.7	2.6 ± 0.2	4.91 ± 0.25
PLA-Gr	45/-45	3972 ± 260	47.5 ± 1.4	49.0 ± 2.8	1.5 ± 0.2	7.20 ± 0.31

Table 1: Mechanical properties for FFF printed PLA and PLA-Gr. E: Young's modulus; σ_y: yield stress; σ_u: ultimate tensile strength; ε_u: strain under maximum load; K_{mat}: fracture toughness.

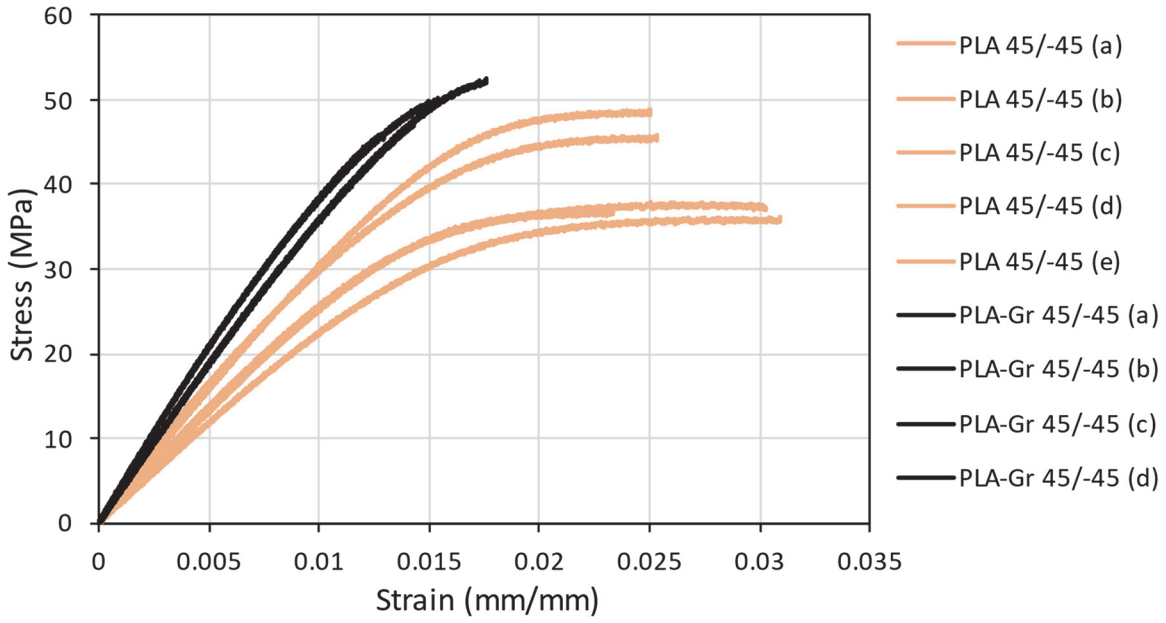

Figure 1: Tensile curves obtained for PLA and PLA-Gr.

A total of 78 plates were tested in this study, encompassing various notch configurations. The plates were classified as U-notched and V-notched, and their geometries and dimensions varied as shown in the scheme of Fig. 2. Here it is important to mention that notches were machined instead of being printed, with the aim of achieving superior finishing and avoid undesirable filament orientation effects during the fracture process [19]. Tabs. 2 and 3 gather the main dimensions (measured values) of the specimens composing the experimental campaign performed in this work.
For U-notched plates, the specimens and nominal dimensions were as follows:

- 12 PLA plates with W=60 mm, a=30 mm (a/W=0.50), with 2 different thicknesses (5 mm and 10 mm) and 2 different notch radii (0.9 mm or 1.3 mm).
- 15 PLA plates with W=120 mm, a=30 mm (a/W=0.25), with 2 different thicknesses (5 mm, 10 mm, and 20 mm) and 2 different notch radii (0.9 mm or 1.3 mm).
- 12 PLA-Gr plates with W=60 mm, a=30 mm (a/W=0.50), with 2 different thicknesses (5 mm and 10 mm) and 2 different notch radii (0.9 mm or 1.3 mm).
- 15 PLA-Gr plates with W=120 mm, a=30 mm (a/W=0.25), with 2 different thicknesses (5 mm, 10 mm, and 20 mm) and 2 different notch radii (0.9 mm or 1.3 mm).

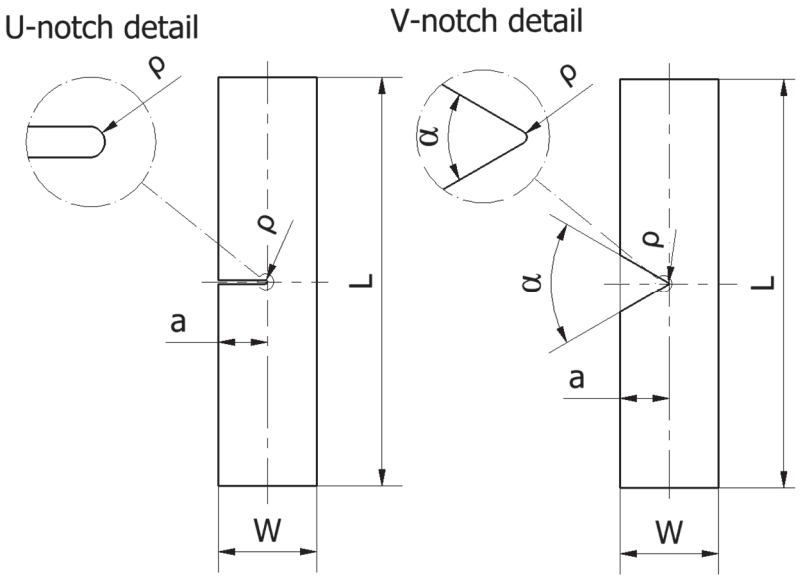

Figure 2: Geometry of the tested plates. ρ: notch radius; a: crack length; W: width; α: notch opening angle; L: length.

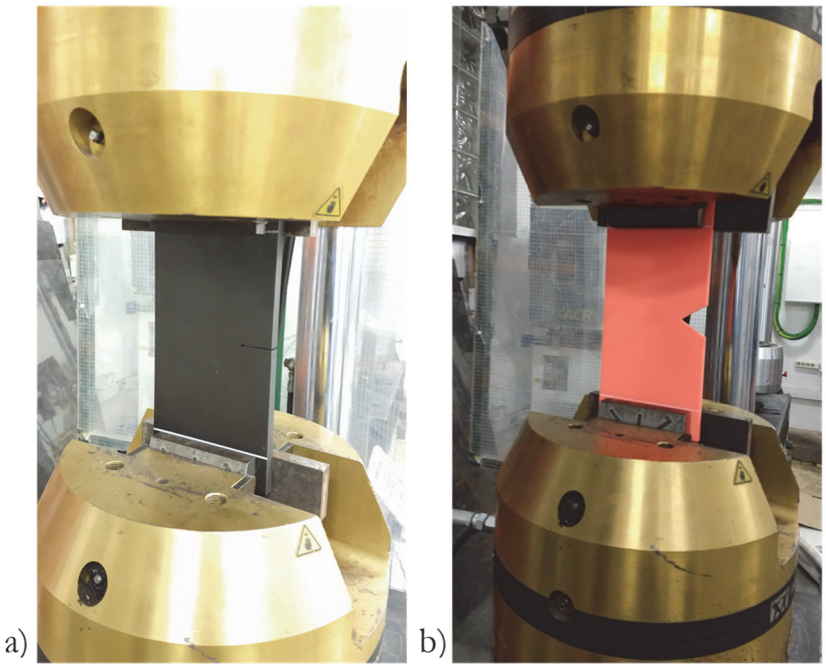

Figure 3: Experimental setup of two of the experiments: a) U-notch, a/W=0.25mm, notch radius=0.9 mm, thickness=10 mm; b) V-notch, a/W=0.25 mm, thickness=5 mm.

Structural detail	Specimen	B (mm)	W (mm)	a (mm)	Notch radius (mm)	P_{EXP} (kN)
U-notch	P201	5.38	60.67	30.65	0.85	3.79
U-notch	P202	4.88	60.66	30.63	0.94	3.98
U-notch	P203	4.89	60.66	30.57	0.94	4.22
U-notch	P204	10.22	60.81	30.16	0.89	9.06
U-notch	P205	10.00	60.78	30.69	0.90	8.44
U-notch	P206	10.01	60.78	30.77	0.89	8.87
U-notch	P207	4.82	120.66	30.42	0.90	13.34
U-notch	P208	4.92	120.56	30.69	0.89	12.53
U-notch	P209	4.89	120.64	30.64	0.84	11.87
U-notch	P210	9.98	120.38	30.50	0.93	23.53
U-notch	P211	9.95	120.34	30.66	0.92	22.19
U-notch	P212	9.97	120.38	30.67	0.94	24.26
U-notch	P213	20.30	120.64	30.42	0.89	44.63
U-notch	P214	20.30	120.64	30.42	0.89	43.62
U-notch	P215	20.30	120.64	30.42	0.89	46.72
U-notch	P301	4.82	60.70	30.63	1.32	3.93
U-notch	P302	4.85	60.65	31.10	1.37	3.98
U-notch	P303	4.94	60.64	30.74	1.29	3.97
U-notch	P304	9.91	60.61	30.69	1.30	8.39
U-notch	P305	9.86	60.62	30.57	1.33	7.56
U-notch	P306	10.00	60.74	31.11	1.30	8.52
U-notch	P307	4.83	120.54	30.76	1.31	12.80
U-notch	P308	4.84	120.65	30.78	1.32	13.48
U-notch	P309	4.93	120.74	30.85	1.31	12.23
U-notch	P310	9.93	120.61	30.77	1.33	23.86
U-notch	P311	9.84	120.40	31.11	1.31	24.36
U-notch	P312	9.88	120.44	30.84	1.31	25.02
V-notch	P401	4.84	60.72	26.95	1.14	3.37
V-notch	P402	4.91	60.76	27.02	1.29	3.49
V-notch	P403	4.90	60.87	27.16	1.58	3.45
V-notch	P404	10.06	60.82	33.00	2.62	8.04
V-notch	P405	9.93	60.61	32.94	3.43	8.32
V-notch	P406	9.98	60.64	26.83	0.84	9.34
V-notch	P407	4.89	120.63	26.81	1.05	11.10
V-notch	P408	5.01	120.64	26.87	0.93	11.04
V-notch	P409	4.75	120.60	26.82	1.04	11.06
V-notch	P410	9.95	120.52	26.81	0.95	28.59
V-notch	P411	9.99	120.48	26.68	0.93	30.10
V-notch	P412	9.95	120.56	26.97	0.75	26.06

Table 2: Test matrix and experimental results for PLA plates.

Structural detail	Specimen	B (mm)	W (mm)	a (mm)	Notch radius (mm)	P_{EXP} (kN)
U-notch	G201	4.85	60.51	30.60	0.86	3.88
U-notch	G202	4.88	60.38	30.84	0.91	3.87
U-notch	G203	4.85	60.50	30.73	0.83	3.89
U-notch	G204	10.02	60.46	30.66	0.87	8.53
U-notch	G205	9.96	60.46	30.59	0.88	8.54
U-notch	G206	9.98	60.49	30.83	0.86	8.77
U-notch	G207	4.96	120.36	31.02	0.81	10.55
U-notch	G208	4.98	120.31	30.34	0.83	13.15
U-notch	G209	4.97	120.20	30.58	0.89	10.15
U-notch	G210	10.14	120.36	31.02	0.89	24.44
U-notch	G211	10.13	120.43	30.92	0.84	26.41
U-notch	G212	10.00	120.48	31.06	0.88	23.08
U-notch	G213	20.17	120.43	31.08	0.88	39.91
U-notch	G214	20.05	120.62	31.25	0.89	42.56
U-notch	G215	20.14	120.63	30.83	0.87	47.30
U-notch	G301	4.86	60.48	30.85	1.24	3.69
U-notch	G302	4.91	60.40	30.98	1.24	4.29
U-notch	G303	4.77	60.54	30.91	1.26	3.81
U-notch	G304	9.96	60.47	30.85	1.26	8.63
U-notch	G305	9.92	60.55	31.19	1.27	8.60
U-notch	G306	9.93	60.47	30.95	1.25	8.40
U-notch	G307	4.88	120.32	30.62	1.26	11.52
U-notch	G308	4.92	120.30	30.93	1.27	11.22
U-notch	G309	4.94	120.42	30.92	1.26	11.47
U-notch	G310	9.96	120.25	31.02	1.27	25.37
U-notch	G311	9.93	120.33	31.04	1.26	22.38
U-notch	G312	9.93	120.43	31.08	1.26	26.32
V-notch	G401	4.76	60.56	27.03	1.25	4.28
V-notch	G402	4.80	60.54	26.87	1.05	4.09
V-notch	G403	4.83	60.49	26.99	0.89	4.59
V-notch	G404	9.92	60.60	26.95	0.65	9.56
V-notch	G405	9.99	60.55	26.92	0.93	10.04
V-notch	G406	9.92	60.58	26.93	0.87	8.76
V-notch	G407	4.89	120.24	26.95	1.07	10.65
V-notch	G408	4.83	120.26	26.50	1.15	10.31
V-notch	G409	4.86	120.33	26.80	1.01	12.06
V-notch	G410	9.94	120.46	26.96	0.97	24.25
V-notch	G411	9.95	120.29	26.92	0.89	25.33
V-notch	G412	9.95	120.53	26.87	1.05	24.11

Table 3: Test matrix and experimental results for PLA-Gr plates.

Additionally, for V-notched plates, the specimens and nominal dimensions were as follows:

- 6 PLA plates with W=60 mm, a=30 mm (a/W=0.50), with 2 different thicknesses (5 mm and 10 mm) and a notch radius (1.3 mm).
- 6 PLA plates with W=120 mm, a=30 mm (a/W=0.25), with 2 different thicknesses (5 mm and 10 mm) and a notch radius (1.3 mm).
- 6 PLA-Gr plates with W=60 mm, a=30 mm (a/W=0.50), with 2 different thicknesses (5 mm and 10 mm) and a notch radius (1.3 mm).
- 6 PLA-Gr plates with W=120 mm, a=30 mm (a/W=0.25), with 2 different thicknesses (5 mm and 10 mm) and a notch radius (1.3 mm).

The displacement rate for all the tensile tests was maintained at 1 mm/min, and the load-displacement curves were recorded until the corresponding critical (maximum) load for each test was reached. Tabs. 2 and 3 gather the obtained critical loads, whereas Fig. 3 shows the experimental setup for both types of notches: a) PLA V-notch plate; b) PLA-Gr U-notch plate. Once the experimental critical loads were determined, the ASED criterion was applied with the aim of estimating the critical loads derived from this approach. The ASED criterion is based on the Strain Energy Density averaged over a control volume surrounding the notch tip. In plane problems, the control volume becomes a circle or a circular sector with radius R_c in the case of V-notches [8] (see Fig. 4).

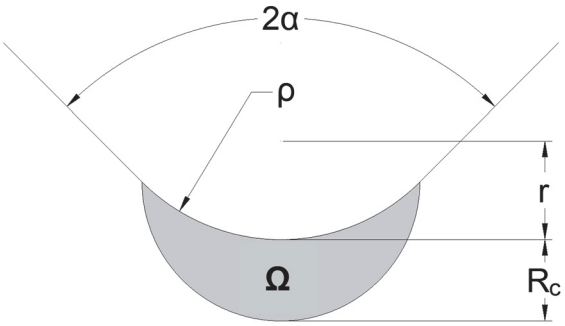

Figure 4: Control area for blunt V-notch. The notch becomes U-notched when α=0.

The SED approach assumes that fracture takes place when the average value of the elastic strain energy ($\bar{W}$) referred to a control volume (or area) is equal to the critical value (W_c), which is a material property. The criterion, thus, may be expressed by Eqn. (1):

$$\bar{W}=W_c \tag{1}$$

According to [20], if the material is ideally brittle, the value of the critical average strain energy density corresponds to the area below the curve of a tensile test, thus following Eqn. (2):

$$W_c=\frac{\sigma_u^{\,2}}{2E} \tag{2}$$

where σ_u is the ultimate tensile strength and E is the Young's Modulus. When the notch opening angle is zero (2α=0), as it is the case for U-notches, the material critical radius R_c can be expressed in terms of the fracture toughness (K_{mat}), the ultimate tensile strength (σ_u), and Poisson's ratio (υ) [21], as shown in Eqns. (3) and (4). The choice between these conditions depends on the material's fracture resistance: when K_{mat} is lower than Eqn. (5) [7], plane strain domains, while plane stress condition is reached when K_{mat} is higher than the value defined by Eqn. (6) [7]. For situations where fracture resistance falls between the values defined by these equations, an interpolation of Eqns. (3) and (4) is required to obtain R_c.

$$R_c=\frac{(1+\upsilon)(5-8\upsilon)}{4\pi}\left(\frac{K_{mat}}{\sigma_u}\right)^2 \qquad \text{Plane strain} \tag{3}$$

$$R_c=\frac{(5-3\upsilon)}{4\pi}\left(\frac{K_{mat}}{\sigma_u}\right)^2 \quad \text{Plane stress} \quad (4)$$

$$K_{mat}=\sigma_y\left(\frac{B}{2.5}\right)^{1/2} \quad \text{Plane strain limit} \quad (5)$$

$$K_{mat}=\sigma_y(\pi B)^{1/2} \quad \text{Plane stress onset} \quad (6)$$

In the case of blunt notches, again the case analyzed in this work, the total strain energy can be determined over the crescent shape volume (Fig. 4) and then the average value of the SED can be expressed in terms of the elastic maximum notch stress (σ_{max}) [8,22]. By applying this condition, the total strain energy density can be obtained over the area Ω (Fig. 3), and the corresponding average value (ASED) follows Eqn. (7) [8]:

$$\bar{W}=F(2\alpha)H\left(2\alpha,\frac{R_C}{\varrho}\right)\frac{\sigma_{max}^{\ 2}}{E} \quad (7)$$

where F(2α) depends on the notch opening angle (0.785 when 2α=0º and 0.662 when 2α=60º), H varies with the notch geometry (2α, R_c/ϱ) and σ_{max} is the maximum elastic stress at the notch tip. The values of the H function for V-shaped notches may be found in [8]. Tab. 4 gathers different values of the H function depending on the notch opening angle and the Poisson's coefficient [8].

2α(rad)	R_c/ϱ	ν =0.3	ν =0.35	ν =0.4
0	0.01	0.5638	0.5432	0.5194
	0.05	0.5086	0.4884	0.4652
	0.1	0.4518	0.4322	0.4099
	1	0.1314	0.1217	0.1110
π/6	0.01	0.6395	0.6162	0.5894
	0.05	0.5760	0.5537	0.5280
	0.1	0.5107	0.4894	0.4651
	1	0.1428	0.1333	0.1226
π/4	0.01	0.6609	0.6369	0.6093
	0.05	0.5945	0.5717	0.5454
	0.1	0.5264	0.5048	0.4802
	1	0.1447	0.1355	0.1252
π/3	0.01	0.6678	0.6436	0.6157
	0.05	0.5998	0.5769	0.5506
	0.1	0.5302	0.5087	0.4842
	1	0.1435	0.1349	0.1252

Table 4: Values of the function H for blunted V-shaped notches [8].

It is important to note that the H values presented in Tab. 4 were tabulated for R_c/ϱ values within a range of 0.01 to 1. Therefore, in order to obtain H values beyond this range it is necessary to extrapolate a fitting curve as proposed in [23]:

$$H=\frac{a}{\frac{R_c}{\varrho}+b} \tag{8}$$

The parameters a and b represent the coefficients required for the fitting curve. In the context of the materials investigated in this study, the curve was fitted utilizing the least-squares methodology, considering a Poisson's ratio of 0.3. The resultant fitting parameters were determined to be 0.1896 and 0.3258 for U-notches, and 0.208 and 0.2982 for V-notches, as illustrated in Fig. 5.

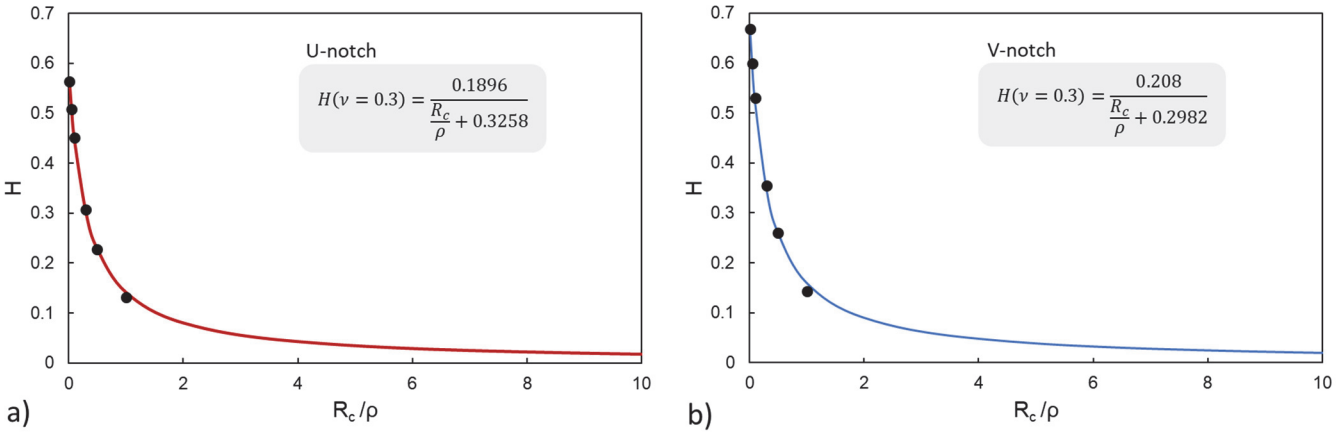

Figure 5: Extrapolated values of the function H for ν=0.3 of a) U-notches and b) V-notches.

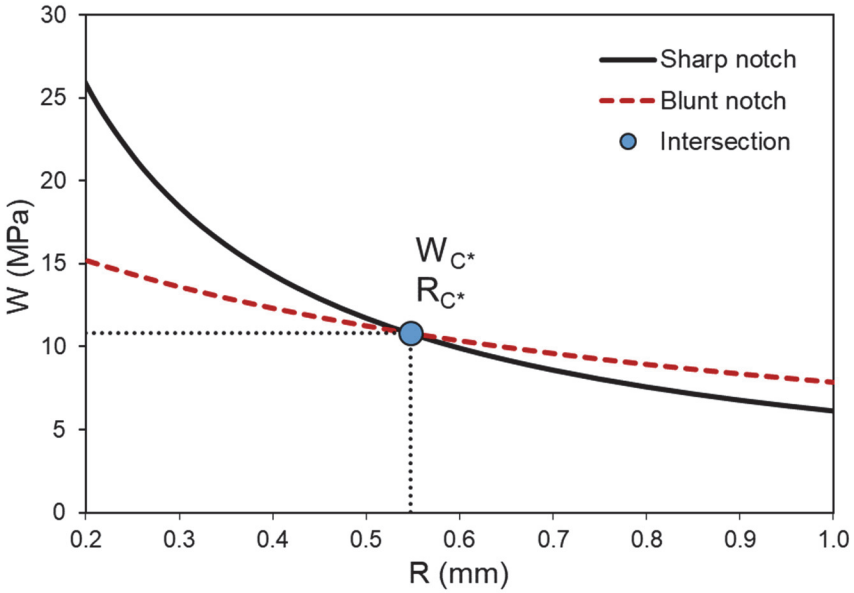

Figure 6: Example of calibration of W_c and R_c parameters with SENB specimens.

When the material being analyzed does not have linear-elastic behavior, the application of the ASED criterion requires a calibration of the material ASED parameters, W_c^* and R_c^* (e.g. [14,24]), accounting for the material non-linearity. Then, the linear-elastic ASED criterion is applied to an equivalent linear-elastic material whose ASED parameters are those obtained from the calibration. The calibration performed here is based on the fracture loads of conventional fracture specimens (e.g., CT or SENB) containing U-notches with different notch radii. With the fracture loads of these two conditions (and the resulting maximum stresses at their corresponding notch tip, σ_{max1} and σ_{max2}), the following conditions may be established:

$$F(2\alpha=0)\cdot H_1\left(2\alpha=0,\frac{R_c}{\varrho_1}\right)\cdot\frac{\sigma_{max1}^{\ 2}}{E}=W_c \tag{9}$$

$$F(2\alpha=0)\cdot H_2\left(2\alpha=0,\frac{R_c}{\varrho_2}\right)\cdot\frac{\sigma_{max2}^{\ 2}}{E}=W_c \tag{10}$$

By introducing different values of R_c in (9) and (10), two W_c vs R_c curves are generated (see Fig. 6). The crossing point of both curves provides the calibrated values of W_c and R_c (W_c* and R_c*).

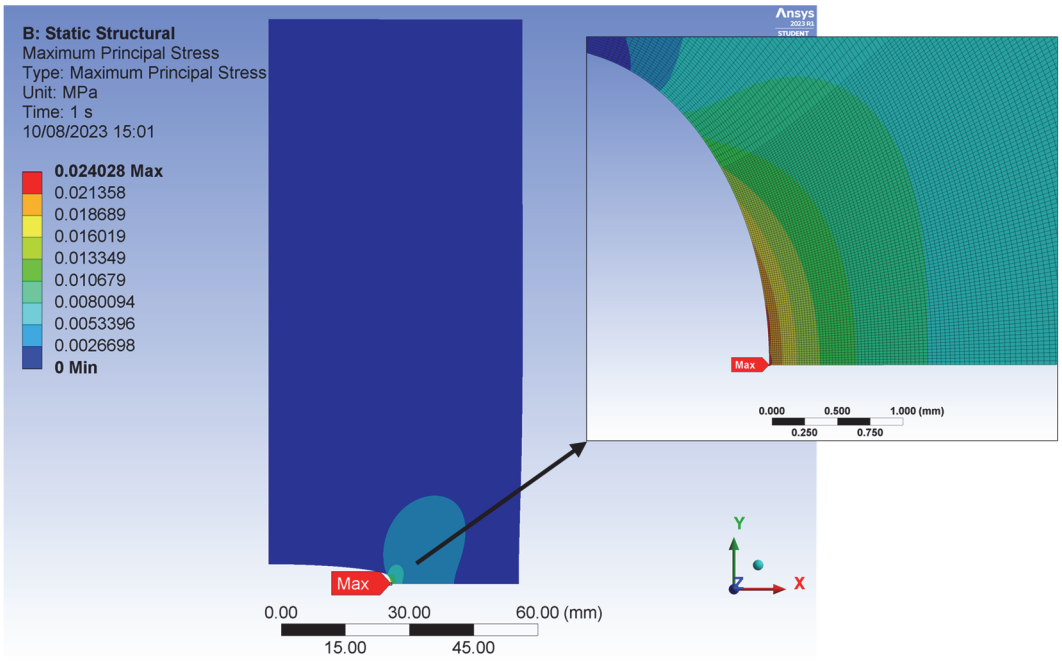

Figure 7: Example of FE model (P306). U-notched specimen, notch radius 1.3 mm, thickness 10 mm. Applied load = 1 N.

Once the calibrated parameters are defined, the fracture load predictions (P_{ASED}) for any other notch radius can be easily derived using the conventional linear-elastic ASED procedure. Based on the failure criterion established by the ASED and using Eqns. (1), (2), and (7), the maximum (critical) stress at the notch tip can be simply derived from the H fitted curve and the mechanical properties of the material:

$$\sigma_{max,\,ASED}=\sqrt{\frac{W_c\cdot E}{F(2\alpha)\cdot H\left(2\alpha,\frac{R_c^{\,*}}{\varrho}\right)}} \tag{11}$$

Thus, the application of this approach requires the definition of the maximum principal stress at the notch tip. With this aim, the different specimens were modeled on finite element (FE) (Ansys) using a half model exploiting the symmetry of the tensile tests, as shown Fig. 7. For each specimen, a 2D plane-stress model with 20-node hexahedric elements and linear-elastic behavior (see Tab. 1) was created. The mesh became more refined as it approached the tip of the notch as the stress is highly sensitive to the mesh size. The maximum principal stress at the notch tip ($\sigma_{max,\,FEA}$) was determined for an arbitrary external tensile load (P_{FEA}=1 N in this case). Then, the critical load was determined applying proportionality conditions by applying Eqn. (12). Here, it is important to note that, given that the stress field may be overly sensitive to the specimen geometry (specially the notch radius), and provided the actual values of the geometrical parameters may differ moderately from the nominal values, the simulation was performed for every single real tested specimen.

$$P_{ASED} = \frac{\sigma_{max,\,ASED}}{\sigma_{max,\,FEA}} \times P_{FEA} \quad (12)$$

RESULTS AND DISCUSSION

In order to better understand the effectiveness of graphene addition in the enhancement of the mechanical behavior of the PLA, one can analyze the results of the tensile tests shown in the Fig. 1 (and Tab. 1), thoroughly analyzed in previous works [15,18]. The main observation is that the introduction of graphene resulted in a notable increase in material brittleness alongside enhanced strength. Concerning the fracture toughness, the addition of graphene also generates a significant improvement of the PLA resistance in the presence of crack-like defects (see Tab. 1).

Moreover, as shown in the load-displacement curves presented in Fig. 8a for SENB cracked and notched specimens (tested in previous experimental programs [15]), the inclusion of growing notches (e.g., 0.25, 0.5, or 1 mm) leads to increased material rigidity in both PLA and PLA-Gr. However, when comparing the load-bearing capacity of the two materials, it remains relatively unchanged in notched conditions, and it clearly increases in cracked conditions when adding graphene (in agreement with the higher K_{mat} reported in Tab. 1). This justifies why PLA-Gr notched plates and PLA notched plates have very similar critical loads for the same geometrical conditions, as shown in Tabs. 2 and 3 and in the examples gathered in Fig. 8b, confirming that the impact of graphene on the load-bearing capacity of notched parts is marginal.

The results shown in Tabs. 2 and 3 also reveal a very minor effect of the notch radius in the notched plates, something that again may be explained from the results obtained in [15] for SENB specimens. Fig. 9a shows the evolution of the (apparent) fracture toughness measured in PLA and PLA-Gr for different notch radii. Interestingly, the addition of graphene affects the toughness at small notch radii, and particularly at cracked conditions, and the notch effect is negligible in both PLA and PLA-Gr for notch radii around 1 mm or higher.

In other words, the results obtained in the notched plates revealed very minor effects of graphene addition and notch radius, and this is justified from the fact that: 1) graphene affects the fracture behavior in cracked conditions or very small notch radii and; 2) the notch effect in these two materials saturates at values of notch radius around 1 mm, with the (nominal) notch radii introduced in the plates being 0.9 mm and 1.3 mm.

In order to assess the efficiency of the suggested ASED calibration, fracture load estimations were first derived by directly employing the traditional ASED criterion (i.e., the linear-elastic approach). A comparison between fracture load predictions obtained using the ASED criterion and actual experimental data is shown in Fig. 10 (also gathered in Tab. 6 of Appendix A). It can be observed that the fracture load estimations using the ASED criterion are considerably lower than the actual experimental fracture loads for the PLA. In this case, the ASED criterion exhibits a clear over-conservatism, with a mean ratio of P_{ASED}/P_{EXP} of 0.63, resulting in poor predictive accuracy. This discrepancy may be attributed to the application of a linear-elastic approach to a material that exhibits a clear non-linear behavior in both tensile and fracture tests, as can be observed in Figs. 1 and 8. Consequently, the estimated critical values derived by the ASED criterion do not accurately represent the actual critical conditions.

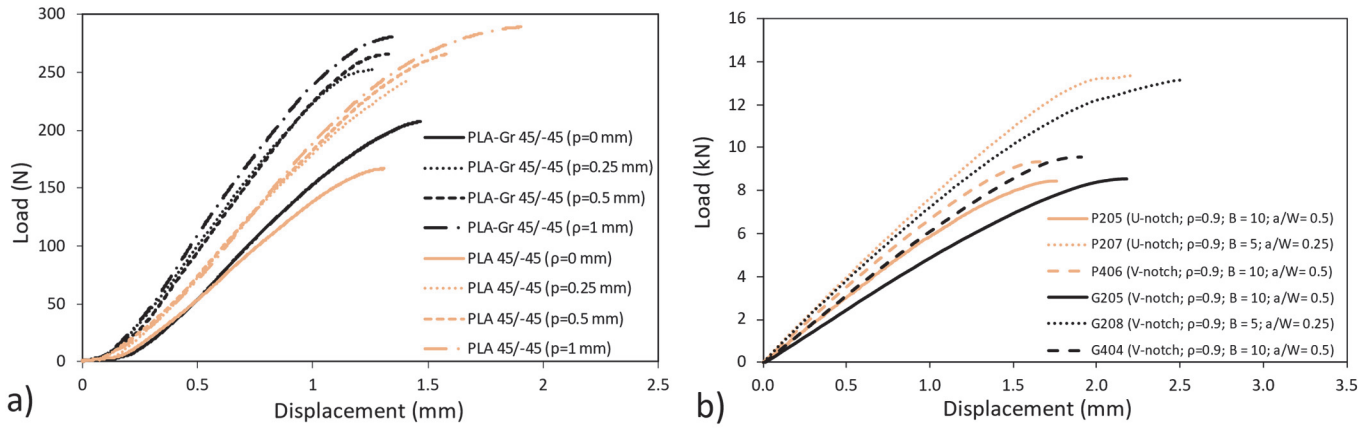

Figure 8: Load displacement curves in PLA and PLA-Gr of a) SENB cracked and notched specimens [15] and b) notched plates.

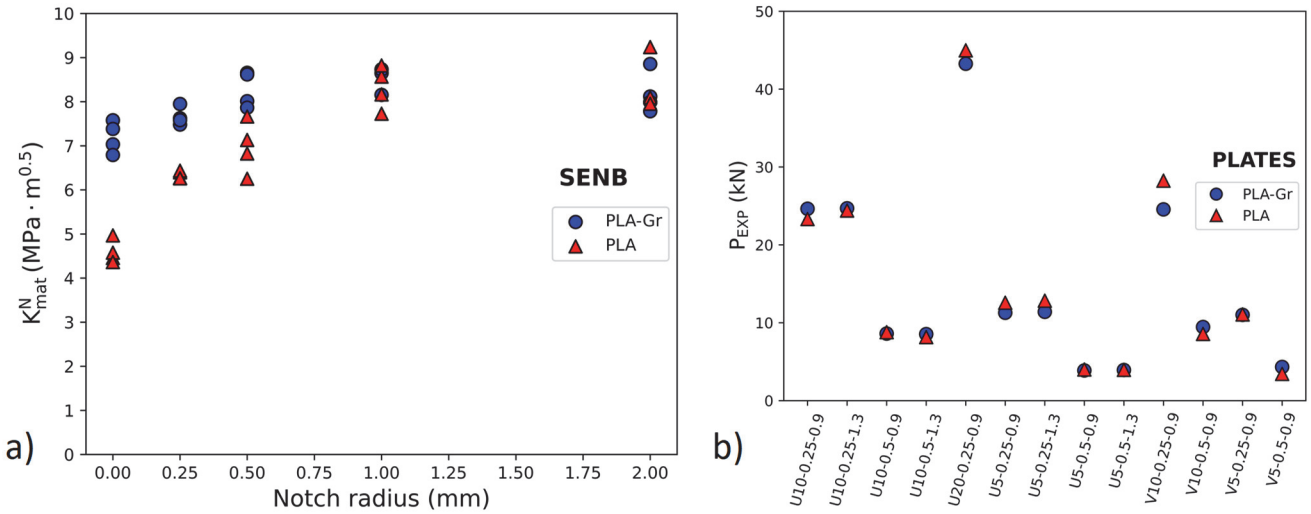

Figure 9: Effect of graphene reinforcement and notch effect in: a) apparent fracture toughness in SENB specimens, and b) experimental critical loads in plates.

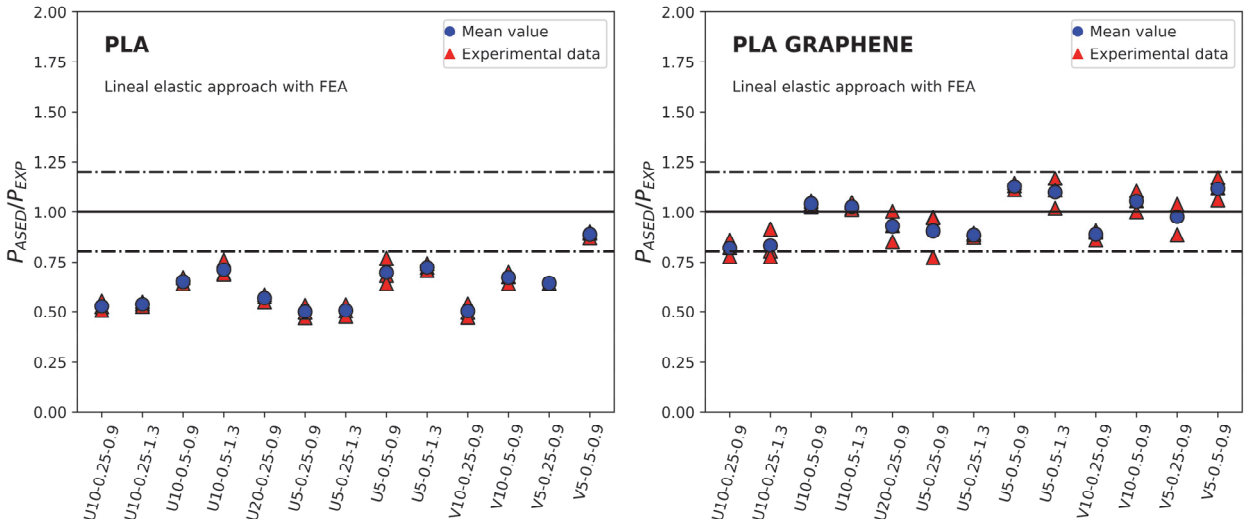

Figure 10: Comparison between fracture load predictions using conventional (linear elastic) ASED criterion (P_{ASED}) and experimental fracture load (P_{EXP}).

On the other hand, when the linear-elastic ASED criterion is directly applied to the PLA-Gr material, the predictions were in very good agreement with the experimental loads, as seen Fig. 10. All the mean values of P_{ASED}/P_{EXP} are within a scatter band of ±20%, which is generally accepted in fracture research [9,25,26], with an overall average underestimation of 2.4%. These findings are explained by the results obtained in the tensile tests shown in Fig. 1 and the proper fracture tests of the plates shown in Fig. 8b, where the amount of non-linearity is very limited, and therefore the liner elastic ASED criterion may capture the real behavior of the material.

Given the limited accuracy exhibited by the linear-elastic approach of the ASED criterion when applied to pristine PLA, it becomes evident the necessity to formulate an alternative method capable of providing more accurate estimations in scenarios where non-linearity is not negligible. Considering this, the outcomes of the calibration for the ASED parameters, as described in the previous section, are presented below. The calibration performed in this work has been based on fracture tests performed on U-notched SENB specimens with notch radii of 0.25 mm (ρ_1) and 1.0 mm (ρ_2), whose details may be found in [15], for the two materials studied. The W curve was calculated as a function of R based on the experimental fracture loads. Tab. 5 gathers the resulting calibrated parameters, becoming evident that the W_c^* value highly deviates from the linear-elastic critical value W_c proposed in the original procedure, especially in the case of PLA material.

Material	Specimen	W_c (MPa)	W_c^* (MPa)	R_c^* (mm)
PLA	SENB	0.31	4.34	0.60
PLA-Gr	SENB	0.30	1.42	1.30

Table 5: ASED calibrated parameters (W_c^* and R_c^*) per material and specimen, together with the linear-elastic formulation of Wc.

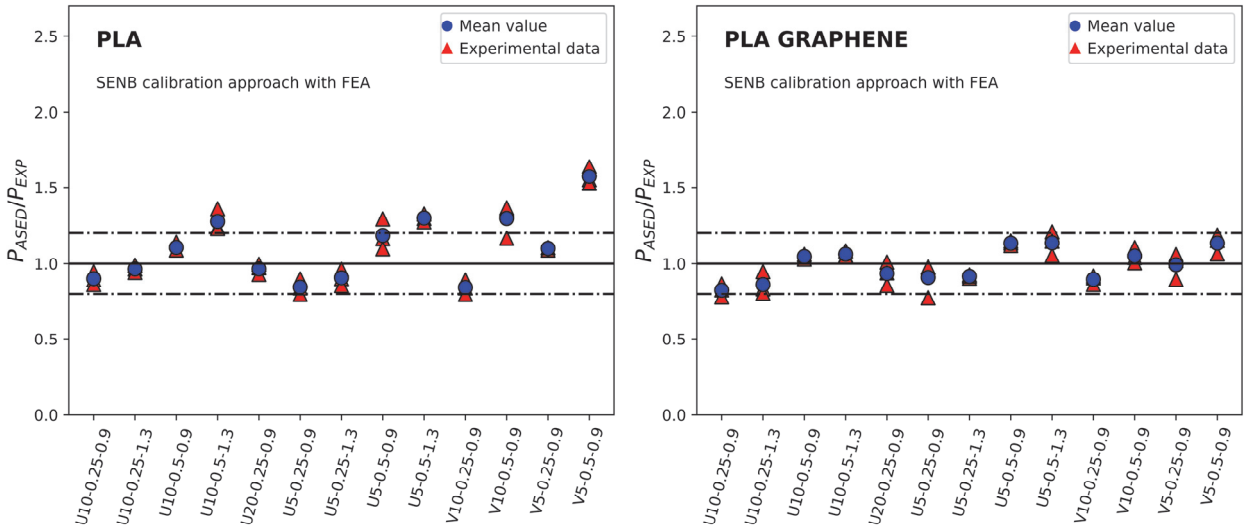

Figure 11: Comparison between the predictions obtained through the calibrated ASED criterion (P_{ASED}) and the experimental critical loads (P_{EXP}).

As illustrated Fig. 11, once the calibration is applied the predictions significantly improved in the case of the notched PLA plates, becoming significantly more accurate, whereas in the case of notched PLA-Gr plates the approach provides similar (but slightly better) results than those obtained without calibration (see Tab. 7 of Appendix A). Now, on average, the P_{ASED}/P_{EXP} ratios are 1.10 and 0.99 for the PLA and PLA-Gr, respectively.

Thus, in general, the results show how the calibrated ASED criterion (in this case, with results obtained on U-notched SENB specimens) provides very good estimations of the fracture loads. Some additional observations can be made when the calibration is performed:

- The thickness has a certain effect on the resulting P_{ASED}/P_{EXP} ratios. The mean value for a nominal thickness of 5 mm is 1.15 and 1.04 for PLA and PLA-Gr, respectively. Similarly, for a thickness value of 10 mm, the average ratio is 1.06 and 0.96 for PLA and PLA-Gr, respectively. Finally, for a thickness value of 20 mm, the mean P_{ASED}/P_{EXP} ratios are 0.97 and 0.96 for PLA and PLA-Gr.
- P_{ASED}/P_{EXP} ratios exhibit comparable values for notch radii of approximately 0.9 mm and 1.3 mm. The average ratios for PLA and PLA-Gr are 1.09 and 0.99, respectively, for 0.9 mm notch radius, and 1.11 and 0.99 for 1.3 mm notch radius, respectively. This implies that the calibrated ASED criterion has been able to predict the negligible notch effect observed in the plates for these particular materials.
- P_{ASED}/P_{EXP} ratios are affected by the length of the notches. The mean P_{ASED}/P_{EXP} ratios for PLA and PLA-Gr are 1.29 and 1.09 (respectively) for a/W =0.50, and 0.93 and 0.90 for a/W=0.25. Then, predictions are resulted more conservative for the shorter defects (a/W=0.25). This may be explained by the fact that the predictions do not consider the constraint conditions in the analysis, whereas in reality, plates with shorter defects are subjected to lower constraint conditions and the notch tip and, thus, may develop higher experimental critical loads (leading to lower P_{ASED}/P_{EXP} ratios).
- The predictions have been generally equally good for U-notches and V-notches, something reasonable considering that Eqn. (7) may be applied to both conditions (actually, a U-notch is a V-notch with α=0°). This being said, there is a clear outlier (V-notch, 5 mm thick plate, a/W=0.5, ρ=0.9 mm) providing an abnormally higher average P_{ASED}/P_{EXP} ratio of 1.57. No reasons have been found for this behavior and requires further analysis in the future.

Conclusions

This paper applies the Average Strain Energy Density (ASED) criterion to estimate the fracture loads in 3D printed PLA and PLA-Gr plates containing different types of notches. All the plates were made by FFF with a single raster orientation (45/-45), and combining different thicknesses, notch geometry (U-notch and V-notch), notch radii and a/W ratios, and were subjected to tensile loading until fracture.

The critical load estimations (P_{ASED}) obtained through the conventional linear-elastic ASED criterion are considerably lower than the experimental ones (P_{EXP}) for PLA plates. In this case, the ratio P_{ASED}/P_{EXP} of 0.63 reveals a clear low accuracy and excessive conservatism. On the other hand, for PLA-Gr plates, the predictions were good, with all the experimental mean values of P_{ASED}/P_{EXP} in the scatter band of ±20%, and an overall slight underestimation of 2.4% (mean P_{ASED}/P_{EXP} ratio close to 0.98). These differences between both materials can be explained due to the limited non-linearity of the PLA-Gr material and the much more significant non-linear behavior of PLA.

Because of the mentioned results, a calibration of the ASED criterion parameters was performed using experimental fracture loads obtained in U-notched SENB specimens with two different notch radii (0.25 mm and 1.0 mm). This calibration accounts for the material non-linearity and provided much better estimations of the fracture loads for the PLA notched plates (with slight improvement for the predictions in PLA-Gr plates). On average, the P_{ASED}/P_{EXP} ratios are 1.10 and 0.99 for the PLA and PLA-Gr, respectively.

Other remarkable observations were the moderate effect of the plate thickness, the minor notch effect observed in the plates and the safer predictions obtained for the shorter defects (a/W=0.25) when compared to the larger ones (a/W=0.50), the latter justified by the different level of constraint.

Overall, the results obtained in this research show that the ASED criterion is capable of providing accurate predictions of critical loads in 3D printed PLA and PLA-Gr notched plates subjected to tensile loads. The obtainment of high accuracy may require, as is the case for non-linear PLA, a previous calibration process.

Acknowledgements

This publication is part of the project “Comportamiento en fractura y efecto entalla en compuestos de matriz termoplástica obtenidos por fabricación aditiva, PID2021-122324NB-I00” funded by MCIN/ AEI /10.13039/501100011033/FEDER “Una manera de hacer Europa”.

References

[1] Cantrell, J.T., Rohde, S., Damiani, D., Gurnani, R., DiSandro, L., Anton, J., Young, A., Jerez, A., Steinbach, D., Kroese, C., Ifju, P.G. (2017). Experimental characterization of the mechanical properties of 3D-printed ABS and polycarbonate parts, Rapid Prototyp. J., 23(4), pp. 811–824. DOI: 10.1108/RPJ-03-2016-0042.

[2] Ahn, S., Montero, M., Odell, D., Roundy, S., Wright, P.K. (2002). Anisotropic material properties of fused deposition modeling ABS, Rapid Prototyp. J., 8(4), pp. 248–257. DOI: 10.1108/13552540210441166.

[3] Ameri, B., Taheri-Behrooz, F., Aliha, M.R.M. (2020). Fracture loads prediction of the modified 3D-printed ABS specimens under mixed-mode I/II loading, Eng. Fract. Mech., 235(May), p. 107181. DOI: 10.1016/j.engfracmech.2020.107181.

[4] Bamiduro, O., Owolabi, G., Haile, M.A., Riddick, J.C. (2019). The influence of load direction, microstructure, raster orientation on the quasi-static response of fused deposition modeling ABS, Rapid Prototyp. J., 25(3), pp. 462–472. DOI: 10.1108/RPJ-04-2018-0087.

[5] Cicero, S., Martínez-Mata, V., Alonso-Estebanez, A., Castanon-Jano, L., Arroyo, B. (2020). Analysis of Notch Effect in 3D-Printed ABS Fracture Specimens Containing U-Notches, Materials (Basel)., 13(21), p. 4716. DOI: 10.3390/ma13214716.

[6] Ng, C.T., Susmel, L. (2020). Notch static strength of additively manufactured acrylonitrile butadiene styrene (ABS), Addit. Manuf., 34(March), p. 101212. DOI: 10.1016/j.addma.2020.101212.

[7] Taylor, D. (2007). The Theory of Critical Distances, Elsevier, DOI: 10.1016/B978-0-08-044478-9.X5000-5.

[8] Berto, F., Lazzarin, P. (2014). Recent developments in brittle and quasi-brittle failure assessment of engineering materials

by means of local approaches, Mater. Sci. Eng. R Reports, 75(1), pp. 1–48. DOI: 10.1016/j.mser.2013.11.001.
[9] Seibert, P., Susmel, L., Berto, F., Kästner, M., Razavi, S.M.J. (2021). Applicability of strain energy density criterion for fracture prediction of notched PLA specimens produced via fused deposition modeling, Eng. Fract. Mech., 258(November), p. 108103. DOI: 10.1016/j.engfracmech.2021.108103.
[10] Sánchez, M., Cicero, S., Arrieta, S., Martínez, V. (2022). Fracture Load Predictions in Additively Manufactured ABS U-Notched Specimens Using Average Strain Energy Density Criteria, Materials (Basel)., 15(7), p. 2372. DOI: 10.3390/ma15072372.
[11] Shahbaz, S., Ayatollahi, M.R., Petru, M., Torabi, A.R. (2022). U-notch fracture in additively manufactured ABS specimens under symmetric three-point bending, Theor. Appl. Fract. Mech., 119. DOI: 10.1016/j.tafmec.2022.103318.
[12] Cicero, S., Torabi, A.R., Majidi, H.R., Gómez, F.J. (2020). On the use of the combined FMC-ASED criterion for fracture prediction of notched specimens with nonlinear behavior, Procedia Struct. Integr., 28(2019), pp. 84–92. DOI: 10.1016/j.prostr.2020.10.011.
[13] Albinmousa, J., AlSadah, J., Hawwa, M.A., Al-Qahtani, H.M. (2021). Estimation of Mode I Fracture of U-Notched Polycarbonate Specimens Using the Equivalent Material Concept and Strain Energy Density, Appl. Sci., 11(8), p. 3370. DOI: 10.3390/app11083370.
[14] Sánchez, M., Cicero, S., Arrieta, S., Torabi, A.R. (2023). Fracture Load Prediction of Non-Linear Structural Steels through Calibration of the ASED Criterion, Metals (Basel)., 13(7), p. 1211. DOI: 10.3390/met13071211.
[15] Cicero, S., Martínez-Mata, V., Castanon-Jano, L., Alonso-Estebanez, A., Arroyo, B. (2021). Analysis of notch effect in the fracture behaviour of additively manufactured PLA and graphene reinforced PLA, Theor. Appl. Fract. Mech., 114, p. 103032. DOI: 10.1016/j.tafmec.2021.103032.
[16] ASTM. (2014). D638-14: Standard Test Method for Tensile Properties of Plastics. DOI: 10.1520/D0638-14.
[17] ASTM. (2000). D6068-10(2018): Standard Test Method for Determining J-R Curves of Plastic Materials. DOI: 10.1520/D6068-10R18.
[18] Cicero, S., Sánchez, M., Martínez-Mata, V., Arrieta, S., Arroyo, B. (2022). Structural integrity assessment of additively manufactured ABS, PLA and graphene reinforced PLA notched specimens combining Failure Assessment Diagrams and the Theory of Critical Distances, Theor. Appl. Fract. Mech., 121, p. 103535. DOI: 10.1016/j.tafmec.2022.103535.
[19] Schmeier, G.E.C., Tröger, C., Kwon, Y.W., Sachau, D. (2023). Predicting Failure of Additively Manufactured Specimens with Holes, Materials (Basel)., 16(6), p. 2293. DOI: 10.3390/ma16062293.
[20] Lazzarin, P., Zambardi, R. (2001). A finite-volume-energy based approach to predict the static and fatigue behavior of components with sharp V-shaped notches, Int. J. Fract., 112(3), pp. 275–298. DOI: 10.1023/A:1013595930617.
[21] Yosibash, Z., Bussiba, A., Gilad, I. (2004). Failure criteria for brittle elastic materials, Int. J. Fract., 125(3–4), pp. 307–333. DOI: 10.1023/b:frac.0000022244.31825.3b.
[22] Seweryn, A. (1994). Brittle fracture criterion for structures with sharp notches, Eng. Fract. Mech., 47(5), pp. 673–681. DOI: 10.1016/0013-7944(94)90158-9.
[23] Justo, J., Castro, J., Cicero, S. (2018). Energy-based approach for fracture assessment of several rocks containing U-shaped notches through the application of the SED criterion, Int. J. Rock Mech. Min. Sci., 110(January), pp. 306–315. DOI: 10.1016/j.ijrmms.2018.07.013.
[24] Seibert, P., Taylor, D., Berto, F., Mohammad Javad Razavi, S. (2022). Energy TCD - robust and simple failure prediction unifying the TCD and ASED criterion, Eng. Fract. Mech., 271. DOI: 10.1016/j.engfracmech.2022.108652.
[25] Chang, K.-Y., Llu, S., Chang, F.-K. (1991). Damage Tolerance of Laminated Composites Containing an Open Hole and Subjected to Tensile Loadings, J. Compos. Mater., 25(3), pp. 274–301. DOI: 10.1177/002199839102500303.
[26] Ibáñez-Gutiérrez, F.T., Cicero, S., Madrazo, V., Berto, F. (2018). Fracture Loads Prediction on Notched Short Glass Fibre Reinforced Polyamide 6 Using the Strain Energy Density, Phys. Mesomech., 21(2), pp. 165–172. DOI: 10.1134/S1029959918020108.

APPENDIX A

Structural detail	Specimen	Lineal elastic		SENB calibration	
		P_{ASED} (kN)	P_{ASED}/P_{EXP}	P_{ASED} (kN)	P_{ASED}/P_{EXP}
U-notch	P201	2.91	0.77	4.90	1.29
U-notch	P202	2.78	0.68	4.74	1.16
U-notch	P203	2.77	0.64	4.73	1.10
U-notch	P204	5.86	0.64	9.93	1.09
U-notch	P205	5.83	0.67	9.89	1.14
U-notch	P206	5.85	0.64	9.91	1.09
U-notch	P207	6.64	0.47	11.26	0.80
U-notch	P208	6.68	0.50	11.30	0.84
U-notch	P209	6.84	0.53	11.51	0.90
U-notch	P210	13.08	0.52	22.26	0.89
U-notch	P211	13.11	0.56	22.30	0.95
U-notch	P212	13.01	0.51	22.18	0.86
U-notch	P213	26.83	0.57	45.42	0.97
U-notch	P214	26.83	0.59	45.42	0.99
U-notch	P215	26.83	0.55	45.42	0.93
U-notch	P301	2.84	0.72	5.09	1.30
U-notch	P302	2.81	0.71	5.07	1.27
U-notch	P303	2.94	0.74	5.26	1.32
U-notch	P304	5.88	0.69	10.52	1.24
U-notch	P305	5.80	0.76	10.41	1.36
U-notch	P306	5.94	0.69	10.61	1.23
U-notch	P307	6.63	0.50	11.87	0.90
U-notch	P308	6.61	0.48	11.84	0.86
U-notch	P309	6.63	0.54	8.51	0.96
U-notch	P310	13.12	0.55	17.22	0.99
U-notch	P311	13.21	0.54	16.77	0.96
U-notch	P312	13.19	0.53	17.01	0.94
V-notch	P401	2.94	0.89	2.88	1.55
V-notch	P402	2.99	0.87	2.98	1.53
V-notch	P403	3.08	0.90	3.10	1.64
V-notch	P404	5.29	0.68	5.02	1.36
V-notch	P405	5.22	0.64	5.35	1.37
V-notch	P406	6.34	0.70	5.65	1.17
V-notch	P407	6.93	0.64	9.26	1.10
V-notch	P408	6.91	0.65	9.26	1.09
V-notch	P409	6.93	0.64	8.97	1.10
V-notch	P410	13.76	0.50	18.49	0.84
V-notch	P411	13.79	0.47	18.57	0.80
V-notch	P412	13.71	0.54	17.71	0.89

Table 6: Critical load predictions for PLA plates.

Structural detail	Specimen	Lineal elastic		SENB calibration	
		P_{ASED} (kN)	P_{ASED}/P_{EXP}	P_{ASED} (kN)	P_{ASED}/P_{EXP}
U-notch	G201	4.54	1.13	4.57	1.13
U-notch	G202	4.42	1.11	4.46	1.12
U-notch	G203	4.62	1.14	4.64	1.15
U-notch	G204	9.26	1.05	9.31	1.06
U-notch	G205	9.21	1.04	9.27	1.05
U-notch	G206	9.29	1.02	9.34	1.03
U-notch	G207	10.61	0.97	10.62	0.97
U-notch	G208	10.46	0.77	10.49	0.77
U-notch	G209	10.14	0.97	10.21	0.98
U-notch	G210	20.28	0.82	20.42	0.83
U-notch	G211	20.79	0.78	20.87	0.78
U-notch	G212	20.33	0.86	20.47	0.87
U-notch	G213	40.82	1.00	41.11	1.01
U-notch	G214	40.71	0.93	41.01	0.94
U-notch	G215	41.16	0.85	41.40	0.86
U-notch	G301	4.38	1.17	4.53	1.21
U-notch	G302	4.42	1.02	4.58	1.05
U-notch	G303	4.27	1.11	4.42	1.15
U-notch	G304	9.17	1.02	9.50	1.05
U-notch	G305	9.12	1.01	9.45	1.05
U-notch	G306	9.20	1.05	9.52	1.08
U-notch	G307	10.19	0.87	10.56	0.90
U-notch	G308	10.15	0.89	10.52	0.93
U-notch	G309	10.17	0.89	10.54	0.92
U-notch	G310	20.19	0.80	20.94	0.83
U-notch	G311	20.30	0.91	21.03	0.95
U-notch	G312	20.30	0.78	21.03	0.81
V-notch	G401	4.64	1.12	4.80	1.15
V-notch	G402	4.65	1.17	4.74	1.19
V-notch	G403	4.71	1.06	4.75	1.06
V-notch	G404	9.79	1.06	9.67	1.04
V-notch	G405	9.73	1.00	9.83	1.01
V-notch	G406	9.37	1.10	9.43	1.10
V-notch	G407	10.38	1.00	10.60	1.02
V-notch	G408	10.36	1.04	10.64	1.06
V-notch	G409	10.35	0.89	10.53	0.90
V-notch	G410	21.12	0.90	21.41	0.91
V-notch	G411	21.13	0.86	21.29	0.86
V-notch	G412	21.16	0.90	21.58	0.92

Table 7: Critical load predictions for PLA-Gr plates.